metals

MDPI

Article

Effect of Process and Post-Process Conditions on the Mechanical Properties of an A357 Alloy Produced via Laser Powder Bed Fusion

Alberta Aversa [1,*], Massimo Lorusso [2], Francesco Trevisan [2], Elisa Paola Ambrosio [2], Flaviana Calignano [2], Diego Manfredi [2], Sara Biamino [1,2], Paolo Fino [1,2], Mariangela Lombardi [1,2] and Matteo Pavese [1]

[1] Department of Applied Science and Technology, Politecnico di Torino, Corso Duca degli Abruzzi 24, 10129 Torino, Italy; sara.biamino@polito.it (S.B.); paolo.fino@polito.it (P.F.); mariangela.lombardi@polito.it (M.L.); matteo.pavese@polito.it (M.P.)

[2] Center for Sustainable Future Technologies—CSFT@POLITO, Istituto Italiano di Tecnologia, Corso Trento 21, 10129 Torino, Italy; massimo.lorusso@iit.it (M.L.); francesco.trevisan@polito.it (F.T.); elisa.ambrosio@iit.it (E.P.A.); flaviana.calignano@iit.it (F.C.); diego.manfredi@iit.it (D.M.)

* Correspondence: alberta.aversa@polito.it; Tel.: +39-01-1090-4763

Academic Editor: Hugo F. Lopez

Received: 25 January 2017; Accepted: 17 February 2017; Published: 22 February 2017

Abstract: A357 samples were realized by laser powder bed fusion (LPBF) on building platforms heated up to different temperatures. The effect of the preheating temperature and of the post processing heat treatment on the microstructure and the mechanical properties of the samples was studied. It was demonstrated that building platform heating can act as an in situ ageing heat treatment following the fast cooling that arises during laser scanning. A 17% higher ultimate tensile strength was achieved by the selection of the optimum building platform temperature. Moreover, the possibility to further increase the mechanical properties by means of a direct ageing heat treatment was investigated.

Keywords: additive manufacturing; aluminum; laser powder bed fusion; A357; mechanical properties; preheating; platform temperature; ageing; cooling rate; selective laser melting

1. Introduction

Additive manufacturing (AM) is defined by the ISO/ASTM 52900:2015 standard as the "process of joining materials to make parts from 3D model data, usually layer upon layer, as opposed to subtractive manufacturing and formative manufacturing methodologies". AM technologies are increasingly employed in the aerospace, automotive and medical fields thanks to the high level of design freedom and the interesting microstructures which can be obtained [1,2]. In fact, these processes allow the production of complex parts which would be difficult or impossible to produce with conventional processes and that would require several manufacturing steps and high material and energy consumption. The ISO/ASTM 52900:2015 standard refers to powder bed fusion (PBF) as the "additive manufacturing process in which thermal energy selectively fuses regions of a powder bed". The laser powder bed fusion (LPBF) process belongs to this class and uses a laser as its energy source. LPBF is one of the most used AM processes, owing to its ability to produce functional near net shape metallic parts with enhanced mechanical properties [3]. Furthermore, LPBF is very attractive thanks to its extremely high cooling rates that can reach 10^6 Ks^{-1} [4], that make it possible, as recently reported in some studies, to obtain metastable structures and supersaturated solid solutions [5–7].

The LPBF process of aluminum and aluminum alloys presents a number of challenges because of its high reflectivity and thermal conductivity and the necessity to use a high quality inert gas

environment during the building process [8,9]. Among commercial aluminum alloys, AlSi10Mg showed to be very suitable for AM technologies due to its composition close to the eutectic one which is responsible for its fine solidification range [10].

A357 is a casting aluminum alloy with a lower silicon content than AlSi10Mg, generally used in the T6 condition [11,12], which has good fatigue and corrosion resistance properties [13]. A357 produced by conventional technologies is generally strengthened by the precipitation hardening through a T6 heat treatment, with a solutionizing at 530–540 °C for 1–12 h followed by quenching in water at room temperature and artificial ageing at 150–225 °C between 3 h and 6 h [11]. This alloy could also be suitable for LPBF as it has a relatively narrow solidification range (65 °C [14]) and a good fluidity in the molten state. The mechanical properties of this alloy are strongly dependent on its microstructural features such as the secondary dendrite arms spacing (SDAS) and the shape and the size of both the eutectic silicon particles and the π-phase ($Al_9FeMg_3Si_5$) [15]. These phases, in fact, have the tendency to crack and have a dramatic effect on the ductility of the alloy. Because of this reason, many studies have been carried out on the selection of the most suitable method that could modify the shape of these phases. The addition of alloying elements (such as Mn, Co, Cr, Sr, Be or Ca) to the A357 is one of the most used techniques to modify the shape of these precipitates [16,17]. However, recent studies have shown that higher cooling rates, compatible with those of LPBF, also produce the change in the morphology of the eutectic Si and Fe-rich particles [17–19].

Up to now, a few studies focused on the microstructure and the properties of A357 samples produced by powder bed AM processes [18,20]. Trevisan et al., for example, evaluated the effect of the post processing heat treatment on the mechanical properties of A357 LPBF and revealed that the as-built condition shows better mechanical performance with respect to both the stress relieved and T6 conditions [20]. Rao et al. studied the influence of LPBF building parameters on the microstructure and the mechanical properties of A357 samples and pointed out that the mechanical properties, strongly depend on both the building direction and the LPBF parameters [18]. Furthermore, the comparison of the microstructure and the mechanical properties of samples built at 35 °C and 200 °C showed that preheating at higher temperatures causes a reduction of the A357 yield and ultimate tensile strengths probably because, in these conditions, an over-ageing phenomenon arises [18].

One important building parameter is the building platform temperature which has an important effect on the microstructure and mechanical properties of LPBF parts [21–23]. In fact, most of the published studies used the platform heating mainly to reduce residual stresses in the part [21,24]. However, it was pointed out that the platform heating also has an important role on the LPBF consolidation phenomena and the microstructure evolution of the processed materials [23]. Buchbinder et al. observed that during the LPBF process of AlSi10Mg, heating the building platform up to 220 °C causes the solidification of a different microstructure, lowering its mechanical properties [22].

In the present work, the building platform temperature for the A357 LPBF process was optimized in order to achieve the most suitable ageing and therefore the highest mechanical properties. Furthermore, the possibility to further increase the mechanical properties by a post processing heat treatment was also investigated.

2. Materials and Methods

An A357 gas atomized powder, with the nominal chemical composition reported in Table 1, provided by LPW Technology (LPW Technology Ltd, Runcorn, UK), was used for LPBF production after its morphology characterization through Field Emission Scanning Electron Microscope (FESEM, SEM-FEG Assing SUPRA 25, Zeiss, Jena, Germany). The FESEM images (Figure 1) show that, generally, particles have a quasi-spherical shape, and many elongated particles are present. As reported in literature, these particles' features could affect the powder flowability and spreading, with consequent defects in final materials [25].

The samples were built using an EOS M270 Dual Mode system (EOS GmbH, Krailling/Munich, Germany) which uses an ytterbium fiber laser with a power up to 200 W. All builds were carried out in

argon atmosphere with 30 µm layer thickness with the EOS stripe scanning strategy [26]. The building parameters, optimized in a previous work [20], are listed in Table 2, where P is the laser power, v is the scan speed, h_d is the hatching distance and S is the stripe length.

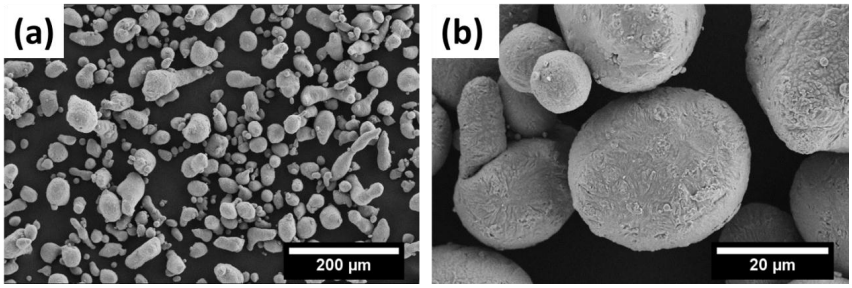

Figure 1. Field Emission Scanning Electron Microscope micrographs of A357 gas atomized particles.

Table 1. Nominal chemical composition of A357 and A356.

Alloy	Si	Mg	Zn	Ti	Cu	Fe	Mn	Al
A357	6.5–7.5	0.45–0.6	<0.05	0.04–0.2	<0.05	<0.1	<0.03	Bal.
A356	6.5–7.5	0.3–0.45	<0.10	<0.20	<0.20	<0.15	<0.10	Bal.

Table 2. Optimized building parameters.

P (W)	v (mm/s)	h_d (mm)	S (mm)
195	1200	0.1	5

Cubic samples with 10 mm size and four tensile samples, in the shape of cylinders, parallel to the building platform, were built varying the platform temperature at 100, 140, 170 and 190 °C. The cubic samples were cut along the building direction, ground and polished to 0.03 µm; then they were etched with a Keller solution for 10 s. Cross-sections were analyzed through FESEM and an optical microscope (Leica DMI 5000 M, Leica Microsystems, Wetzlar, Germany). X-rays measurements were carried out on the cubes' cross-section using a X-Pert Philips diffractometer (PANalytical, Almelo, The Netherland) in a Bragg Brentano configuration in a 2θ range between 20° and 110° (operated at 40 kV and 40 mA with a step size 0.013 and 25 s per step). The precipitation phenomena on the as-built samples were studied by means of a differential thermal analysis (TGA-DTA METTLER Toledo 1600, Mettler Toledo, Greifensee, Switzerland) with a 5 °C/min ramp from 25 to 450 °C.

The cylindrical samples were machined in order to obtain tensile samples with a gauge length and diameter respectively of 40 and 8 mm and tested by a Zwick Z100 tensile machine (Zwick/Roell Ulm, Germany) using 8×10^{-3} s^{-1} as the strain rate. The fracture surfaces of the samples were observed by FESEM microscopy in order to evaluate the failure.

Some cubic samples, realized with different platform temperatures, were then aged up to 5 h at 170 °C in order to study the possibility to further increase the hardness values by means of a post processing heat treatment.

Hardness measurements were carried out on the as-built and aged samples' cross-section using a micro Vickers indenter with a load of 100 g applied for 15 s. Five different indentations were realized on each A357 sample.

3. Results and Discussion

The FESEM micrographs of the samples' cross-sections, illustrated in Figure 2, reveal that in all cases, an extremely fine microstructure, constituted by α-Al cells surrounded by the eutectic, is formed as a consequence of the rapid solidification. No significant microstructural differences can be highlighted among samples built at different temperatures.

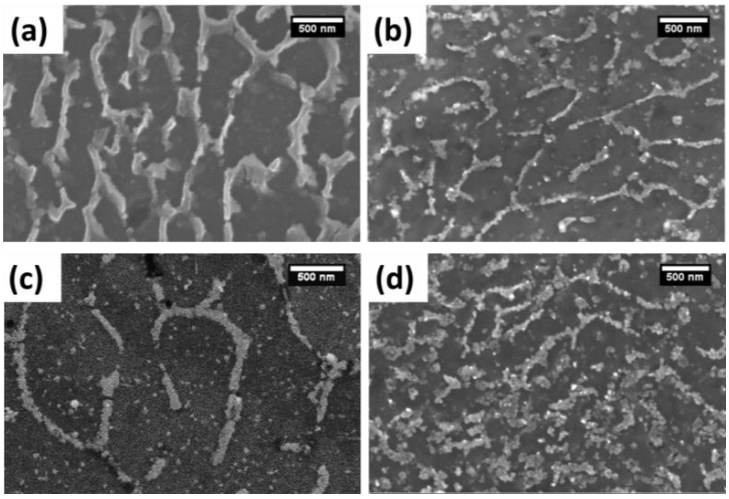

Figure 2. FESEM micrographs of A357 samples' cross-section built at (**a**) 100; (**b**) 140; (**c**) 170; and (**d**) 190 °C.

In Figure 3a, it is possible to note that the X-ray diffraction (XRD) patterns of the samples built at different temperatures are similar. Only a slight increase in the intensity of silicon peaks can be observed in the samples built with higher building platform temperature (Figure 3b). The higher intensity of Si peaks in XRD of the samples built with higher building platform temperatures could be due to further precipitation of Si in the eutectic region at higher building platform temperatures. The silicon moves, in fact, inside the fine eutectic phase [27] (bright regions in Figure 2), from a supersaturated solid solution to Si stables precipitates [18]. Furthermore, no traces of the Mg_2Si strengthening phase were observed in the XRD patterns of the A357 samples built at different temperatures, probably because its relative quantity is lower than the X-ray detection limit.

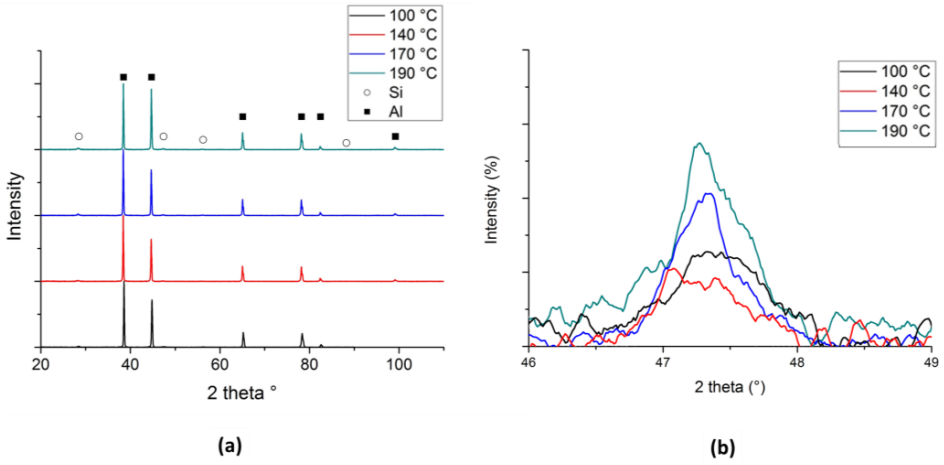

Figure 3. (**a**) X-ray diffraction patterns of the sample cross-sections; and (**b**) detail of Si (111) peaks.

The differential thermal analyses (DTA) measurements reported in Figure 4 allow to make some further considerations on the precipitation of the reinforcing phases. Two exothermic peaks are visible in all the samples. The first peak around 250 °C is imputable to the precipitation of Mg_2Si and the second might be correlated to the diffusional processes of the silicon contained in an α-Al supersaturated solid solution [28,29]. It can be noticed that the higher the building platform temperature, the lower the intensity of the first peak. It is thus reasonable to suppose that samples built at higher temperatures contain more Mg_2Si, whereas the LPBF process carried out at low temperatures

produced materials containing Mg and Si in solid solution. These different conditions in as-built specimens imply a different precipitation level during the DTA measurement. DTA data suggest that higher building platform temperatures allow the Mg_2Si precipitation during the LPBF process and therefore act as an in situ ageing process.

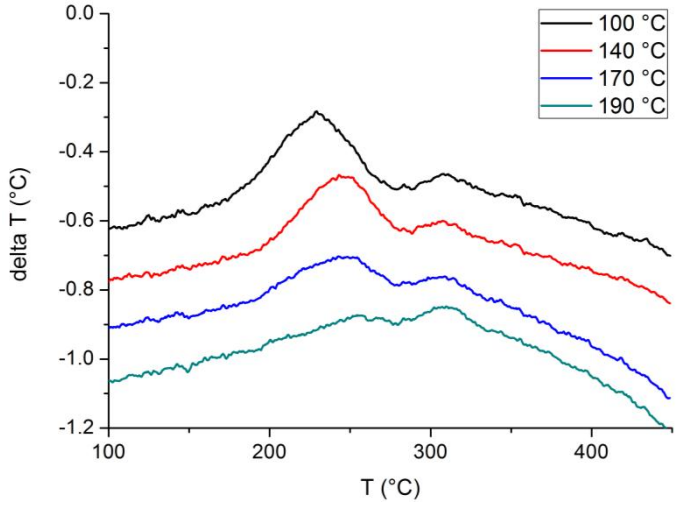

Figure 4. Differential thermal analysis (DTA) measurements of A357 samples produced with different building platform temperatures.

The most representative tensile curves of A357 samples built at different temperatures, reported in Figure 5, confirm the hypothesis concerning precipitate evolution in A357 during LPBF at different platform temperatures. The building platform heating can act as an ageing treatment during the process; therefore, it has an important effect on the mechanical behaviour of the LPBF samples. The mean values of yield strength (σ_y), ultimate tensile strength (UTS) and elongation at break (ε_r), listed in Table 3, show that temperatures of 140 °C and 170 °C produce an increase in σ_y and UTS with respect to the samples obtained at 100 °C. If the platform temperature is further increased to 190 °C, the material strength decreases again to values closer to the ones of the sample built with a platform temperature of 100 °C suggesting that, in this case, an over-ageing process arose. In addition, in Table 3, literature data of A357 alloys produced by LPBF on different building platform temperatures are compared with the results of this work.

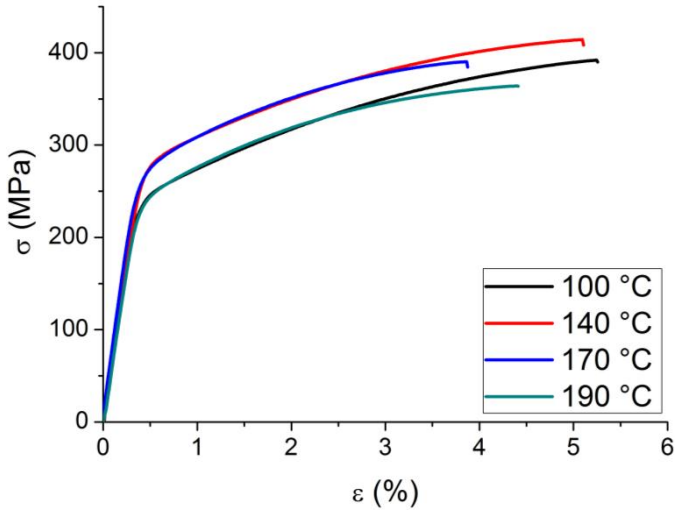

Figure 5. Stress–strain curves of A357 samples.

Rao et al. processed A357 by LPBF using different conditions (different gas atomized powder and building parameters) with respect to those employed in this work [18]. Their materials processed at high platform temperature presented lower strength values than the one described in this paper and, consequently, a higher elongation at break. However, the highest UTS was obtained by Rao et al. on A357 samples built at 35 °C [18].

In addition, in order to evaluate the LPBF potentialities, mechanical properties of A357 and A356 (the composition of which is reported in Table 1) materials produced by conventional technologies and submitted to the T6 post process are also included in Table 3. LPBF samples obtained with controlled building platform temperatures have strength comparable or superior to the best materials obtained by casting and T6. Regarding fracture strain, only thixoforming and T6 guarantees better values than LPBF.

Table 3. Mechanical properties of the A357 samples built with different building platform temperatures.

Alloy	Yield strength σ_y (MPa)	Ultimate Tensile Strength UTS (MPa)	Elongation at Break ε_r (%)
A357 LPBF 100 °C	245 ± 4	389 ± 3	5.2 ± 0.2
A357 LPBF 140 °C	284 ± 3	408 ± 5	4.9 ± 0.2
A357 LPBF 170 °C	288 ± 7	397 ± 9	3.8 ± 0.3
A357 LPBF 190 °C	246 ± 4	362 ± 2	4.4 ± 0.1
A357 LPBF 35 °C [18]	279.6 ± 0.1	426.4 ± 2.6	10.1 ± 0.5
A357 LPBF 200 °C [18]	205.3 ± 1.3	307.7 ± 1.6	10.9 ± 0.7
A357Cast and T6 [16]	281	305	4.1
A356 Rheocast and T6 [30]	150	212	4.7
A356 Thixoform and T6 [30]	290	378	24.5

FESEM micrographs of the A357 fracture surfaces, shown in Figure 6, reveal that, in all the cases, very small dimples are formed, indicating a ductile fracture and confirming the fine microstructure formed during the LPBF process. From the comparison of the fracture surfaces, it can be noticed that a slight widening of the microstructure can be observed only for the material built with a platform temperature of 190 °C.

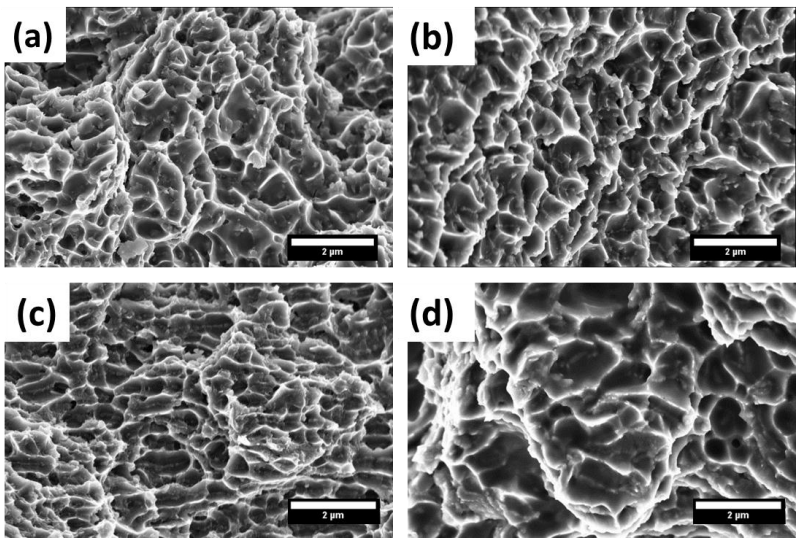

Figure 6. FESEM micrographs of the fracture surface of A357 samples built at (**a**) 100; (**b**) 140; (**c**) 170; and (**d**) 190 °C.

Finally, the possibility to further increase the properties of A357 samples built with different platform temperatures by means of a post processing heat treatment was investigated. An ageing

temperature of 170 °C was selected, based on the results of the T6 optimization of A357 LPBF samples of Trevisan et al. [20].

From the hardness trend of the samples with the ageing time, as shown in Figure 7, it can be noticed that, in the cases of samples obtained with platform temperatures of 100 °C and 140 °C, a significant further increase in the hardness was achieved for treatments up to 3 h. Before ageing, these samples were characterized by a supersaturated solid solution, with traces of Si (Figure 3) precipitates. Starting from this metastable condition, during ageing treatment, precipitation phenomena occur, with a consequent strengthening of the LPBF A357. For samples obtained at 170 °C and 190 °C instead, in which, during the LPBF process more precipitates formed, the heat treatment has little effects for shorter times. In all the cases, for longer treatments, over-ageing is observed, with the corresponding reduction in material hardness. Furthermore, the comparison of the ageing curves also highlights that the hardness values have a different trend with the ageing time depending on the building platform temperature used during the LPBF process. Samples built at 100 °C, for example, reach the maximum hardness value after 3 h at 170 °C, while samples built at 140 °C reach the maximum hardness after 1 h heat treatment; the ageing heat treatment only slightly affects the hardness of samples built at 170 °C and 190 °C. Finally, it is worth noting that the 190 °C hardness values are always lower than all the others. The analysis of the hardness results suggests that it is possible to improve the mechanical performances of A357 built with the platform temperature of 100 °C by applying a heat treatment at 170 °C for 3 h.

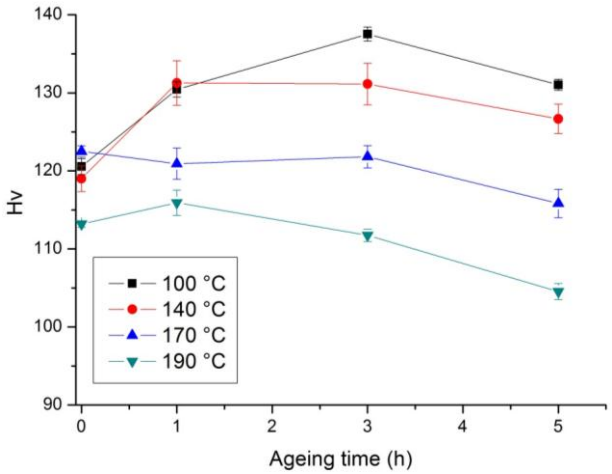

Figure 7. Micro-Vickers hardness values of the A357 samples during direct-ageing treatment at 170 °C.

4. Conclusions

In this work, the effect of the building platform temperature and of post processing heat treatments on the mechanical properties of LPBF A357 samples was investigated. It was reported that the highest mechanical properties are achieved with 140 °C and 170 °C platforms. These results suggest that the high cooling rate that arises during the laser scanning has a quenching effect on the microstructure of the alloy. Therefore, building platform heating can act as an ageing process and induces the precipitation of strengthening phases. The low yield strength values, observed for materials built with platform temperatures of 100 °C and 190 °C could be ascribed to under-ageing and over-ageing respectively, imputable to lower or higher silicon precipitate contents in the alloys. In fact, higher building platform temperatures promote Si diffusion from a supersaturated solid solution to stables precipitates. The metastable phase conditions created through the heating building platform during the LPBF process undergo different evolutions during a heating post process at 170 °C, inducing a change in hardness values depending on the ageing times. The analysis of the

hardness results suggests that it is possible to improve the mechanical performances of A357 built with a platform temperature of 100 °C by applying a heat treatment at 170 °C for 3 h.

Acknowledgments: The authors would like to acknowledge the European research project belonging to the VII framework program AMAZE, Additive Manufacturing Aiming toward Zero Waste and Efficient Production of High-Tech Metal Products.

Author Contributions: Alberta Aversa, Francesco Trevisan built the A357 samples and did the main characterizations. Massimo Lorusso did all mechanical tests. Elisa Paola Ambrosio did the DTA analyses. Flaviana Calignano is responsible for the LPBF process and took part to the writing process. Diego Manfredi did FESEM images and took part to the writing process. Sara Biamino did the XRD analyses. Paolo Fino, Matteo Pavese and Mariangela Lombardi, supervised the whole work and took part to the writing process.

Conflicts of Interest: The authors declare no conflict of interest.

References

1. Olakanmi, E.O.; Cochrane, R.F.; Dalgarno, K.W. A review on selective laser sintering/melting (SLS/SLM) of aluminium alloy powders: Processing, microstructure, and properties. *Prog. Mater. Sci.* **2015**, *74*, 401–477. [CrossRef]
2. Ma, P.; Prashanth, K.; Scudino, S.; Jia, Y.; Wang, H.; Zou, C.; Wei, Z.; Eckert, J. Influence of Annealing on Mechanical Properties of Al-20Si Processed by Selective Laser Melting. *Metals* **2014**, *4*, 28–36. [CrossRef]
3. Abd Malek, N.M.S.; Mohamed, S.R.; Che Ghani, S.A.; Wan Harun, W.S. Critical evaluation on structural stiffness of porous cellular structure of cobalt chromium alloy. *IOP Conf. Ser. Mater. Sci. Eng.* **2015**, *100*, 012019. [CrossRef]
4. Yuan, P.; Gu, D. Molten pool behaviour and its physical mechanism during selective laser melting of TiC/AlSi10Mg nanocomposites: Simulation and experiments. *J. Phys. D Appl. Phys.* **2015**, *48*, 035303. [CrossRef]
5. Li, X.P.; Kang, C.W.; Huang, H.; Zhang, L.C.; Sercombe, T.B. Selective laser melting of an Al86Ni6Y4.5Co2La1.5 metallic glass: Processing, microstructure evolution and mechanical properties. *Mater. Sci. Eng. A* **2014**, *606*, 370–379. [CrossRef]
6. Schmidtke, K.; Palm, F.; Hawkins, A.; Emmelmann, C. Process and Mechanical Properties: Applicability of a Scandium modified Al-alloy for Laser Additive Manufacturing. *Phys. Procedia* **2011**, *12*, 369–374. [CrossRef]
7. Aversa, A.; Lorusso, M.; Cattano, G.; Manfredi, D.; Calignano, F.; Ambrosio, E.P.; Biamino, S.; Fino, P.; Lombardi, M.; Pavese, M. A study of the microstructure and the mechanical properties of an AlSiNi alloy produced via selective laser melting. *J. Alloys Compd.* **2016**, *695*, 1470–1478. [CrossRef]
8. Boschetto, A.; Bottini, L.; Veniali, F. Roughness modeling of AlSi10Mg parts fabricated by selective laser melting. *J. Mater. Process. Technol.* **2017**, *241*, 154–163. [CrossRef]
9. Lorusso, M.; Aversa, A.; Manfredi, D.; Calignano, F.; Ambrosio, E.P.; Ugues, D.; Pavese, M. Tribological Behavior of Aluminum Alloy AlSi10Mg-TiB2 Composites Produced by Direct Metal Laser Sintering (DMLS). *J. Mater. Eng. Perform.* **2016**, *25*, 3152–3160. [CrossRef]
10. Gu, D.; Wang, H.; Dai, D.; Chang, F.; Meiners, W.; Hagedorn, Y.-C.; Wissenbach, K.; Kelbassa, I.; Poprawe, R. Densification behavior, microstructure evolution, and wear property of TiC nanoparticle reinforced AlSi10Mg bulk-form nanocomposites prepared by selective laser melting. *J. Laser Appl.* **2015**, *27*, S17003. [CrossRef]
11. Saboori, A.; Pavese, M.; Badini, C.; Eivani, A.R. Studying the age hardening kinetics of A357 aluminum alloys through the Johnson–Mehl–Avrami theory. *Met. Powder Rep.* **2016**. [CrossRef]
12. Ceschini, L.; Morri, A.; Morri, A.; Gamberini, A.; Messieri, S. Correlation between ultimate tensile strength and solidification microstructure for the sand cast A357 aluminium alloy. *Mater. Des.* **2009**, *30*, 4525–4531. [CrossRef]
13. Es-Said, O.S.; Lee, D.; Pfost, W.D.; Thompson, D.L.; Patterson, M.; Foyos, J.; Marloth, R. Alternative heat treatments for A357-T6 aluminum alloy. *Eng. Fail. Anal.* **2002**, *9*, 99–107. [CrossRef]
14. Zulfia, A.; Atkinson, H.V.; Jones, H.; King, S. Effect of hot isostatic pressing on cast A357 aluminium alloy with and without SiC particle reinforcement. *J. Mater. Sci.* **1999**, *34*, 4305–4310. [CrossRef]
15. Wang, Q.G.; Caceres, C.H.; Griffiths, J.R. Damage by eutectic particle cracking in aluminum casting alloys A356/357. *Metall. Mater. Trans. A* **2003**, *34*, 2901–2912. [CrossRef]

16. Yang, C.Y.; Lee, S.L.; Lee, C.K.; Lin, J.C. Effects of Be and Fe on the mechanical and corrosion behaviors of A357 alloys. *Mater. Chem. Phys.* **2005**, *93*, 412–419. [CrossRef]
17. Dezecot, S.; Brochu, M. Microstructural characterization and high cycle fatigue behavior of investment cast A357 aluminum alloy. *Int. J. Fatigue* **2015**, *77*, 154–159. [CrossRef]
18. Rao, H.; Giet, S.; Yang, K.; Wu, X.; Davies, C.H.J. The influence of processing parameters on aluminium alloy A357 manufactured by Selective Laser Melting. *Mater. Des.* **2016**, *109*, 334–346. [CrossRef]
19. Garcìa-Garcìa, G.; Espinoza-Cuadra, J.; Mancha-Molinar, H. Copper content and cooling rate effects over second phase particles behavior in industrial aluminum-silicon alloy 319. *Mater. Des.* **2007**, *28*, 428–433. [CrossRef]
20. Trevisan, F.; Calignano, F.; Lorusso, M.; Ambrosio, E.P.; Lombardi, M.; Pavese, M.; Manfredi, D. Effects of Heat Treatments on A357 Alloy Produced by Selective Laser Melting. In Proceedings of the World PM 2016, Hamburg, Germany, 9–13 October 2016.
21. Kaufmann, F.; Imran, N.; Wischeropp, M.; Emmelmann, T.; Siddique, C.; Walther, S. Influence of process parameters on the quality of aluminium alloy EN AW 7075 using selective laser melting (SLM). *Phys. Procedia* **2016**, *83*, 918–926. [CrossRef]
22. Buchbinder, D.; Meiners, W.; Wissenbach, K.; Poprawe, R. Selective laser melting of aluminum die-cast alloy—Correlations between process parameters, solidification conditions, and resulting mechanical properties. *J. Laser Appl.* **2015**, *27*, S29205. [CrossRef]
23. Yadroitsev, I.; Krakhmalev, P.; Yadroitsava, I.; Johansson, S.; Smurov, I. Energy input effect on morphology and microstructure of selective laser melting single track from metallic powder. *J. Mater. Process. Technol.* **2013**, *213*, 606–613. [CrossRef]
24. Brandl, E.; Heckenberger, U.; Holzinger, V.; Buchbinder, D. Additive manufactured AlSi10Mg samples using Selective Laser Melting (SLM): Microstructure, high cycle fatigue, and fracture behavior. *Mater. Des.* **2012**, *34*, 159–169. [CrossRef]
25. Spierings, A.B.; Voegtlin, M.; Bauer, T.; Wegener, K. Powder flowability characterisation methodology for powder-bed-based metal additive manufacturing. *Prog. Addit. Manuf.* **2015**, *1*, 9–20. [CrossRef]
26. Manfredi, D.; Calignano, F.; Krishnan, M.; Canali, R.; Ambrosio, E.; Atzeni, E. From Powders to Dense Metal Parts: Characterization of a Commercial AlSiMg Alloy Processed through Direct Metal Laser Sintering. *Materials* **2013**, *6*, 856–869. [CrossRef]
27. Wu, J.; Wang, X.Q.; Wang, W.; Attallah, M.M.; Loretto, M.H. Microstructure and strength of selectively laser melted AlSi10Mg. *Acta Mater.* **2016**, *117*, 311–320. [CrossRef]
28. García-Cordovilla, C.; Louis, E.; Narciso, J.; Pamies, A. A differential scanning calorimetry study of solid state reactions in AA6061/SiC, AA6061/Al2O3 and A357 /SiC composites fabricated by means of compocasting. *Mater. Sci. Eng. A* **1994**, *189*, 219–227. [CrossRef]
29. Fiocchi, J.; Tuissi, A.; Bassani, P.; Biffi, C.A. Low temperature annealing dedicated to AlSi10Mg selective laser melting products. *J. Alloys Compd.* **2017**, *695*, 3402–3409. [CrossRef]
30. Tahamtan, S.; Boostani, A.F.; Nazemi, H. Mechanical properties and fracture behavior of thixoformed, rheocast and gravity-cast A356 alloy. *J. Alloys Compd.* **2009**, *468*, 107–114. [CrossRef]